Accelerated Publications

Structure of a Nitric Oxide Synthase Heme Protein from *Bacillus subtilis*[†,‡]

Kartikeya Pant,[§] Alexandrine M. Bilwes,[§] Subrata Adak,[||] Dennis J. Stuehr,[||] and Brian R. Crane*[,§]

The Department of Chemistry and Chemical Biology, Cornell University, Ithaca, New York 14853, and The Department of Immunology, Lerner Research Institute, The Cleveland Clinic, Cleveland, Ohio 44195

Received June 27, 2002; Revised Manuscript Received July 23, 2002

ABSTRACT: Eukaryotic nitric oxide synthases (NOSs) produce nitric oxide to mediate intercellular signaling and protect against pathogens. Recently, proteins homologous to mammalian NOS oxygenase domains have been found in prokaryotes and one from *Bacillus subtilis* (bsNOS) has been demonstrated to produce nitric oxide [Adak, S., Aulak, K. S., and Stuehr, D. J. (2002) *J. Biol. Chem. 277*, 16167−16171]. We present structures of bsNOS complexed with the active cofactor tetrahydrofolate and the substrate L-arginine (L-Arg) or the intermediate N^{ω}-hydroxy-L-arginine (NHA) to 1.9 or 2.2 Å resolution, respectively. The bsNOS structure is similar to those of the mammalian NOS oxygenase domains ($mNOS_{ox}$) except for the absence of an N-terminal β-hairpin hook and zinc-binding region that interact with pterin and stabilize the $mNOS_{ox}$ dimer. Changes in patterns of residue conservation between bacterial and mammalian NOSs correlate to different binding modes for pterin side chains. Residue conservation on a surface patch surrounding an exposed heme edge indicates a likely interaction site for reductase proteins in all NOSs. The heme pockets of bsNOS and $mNOS_{ox}$ recognize L-Arg and NHA similarly, although a change from Val to Ile beside the substrate guanidinium may explain the 10−20-fold slower dissociation of product NO from the bacterial enzyme. Overall, these structures suggest that bsNOS functions naturally to produce nitrogen oxides from L-Arg and NHA in a pterin-dependent manner, but that the regulation and purpose of NO production by NOS may be quite different in *B. subtilis* than in mammals.

Nitric oxide synthases (NOSs)[1] are highly regulated enzymes that are responsible for the synthesis of the potent cytotoxin and signal molecule nitric oxide (NO) (*1*−*3*). To produce NO, NOSs catalyze the five-electron heme-based oxidation of L-arginine (L-Arg) to L-citrulline (L-Cit) via the stable intermediate N^{ω}-hydroxy-L-arginine (NHA) (*4*). In mammals, NO has many activities that range from protection against pathogens and tumor cells to blood pressure regulation and nerve cell communication (*1*). These protection and signaling functions of NO serve a multicellular organism well. Bacteria also produce NO as an intermediate of denitrification, but the enzymes that are involved are vastly different from eukaryotic NOSs (*5*). Recently, however, NOS-like proteins have been identified in the genome sequences of prokaryotes, consistent with early reports of NOS activity in *Staphylococcus* (*6*) and *Nocardia* (*7*).

Eukaryotic NOSs are found as three homodimeric isozymes: inducible NOS (iNOS), neuronal NOS (nNOS), and endothelial NOS (eNOS). Each NOS isozyme contains a catalytic N-terminal oxygenase domain (NOS_{ox}, residues 1−498 for murine iNOS) that binds heme (iron protoporphyrin IX), tetrahydrobiopterin (H_4B), the substrate L-Arg, and a C-terminal electron-supplying reductase domain (NOS_{red}, residues 531−1144 for iNOS) that is homologous to cytochrome P450 reductase and binds flavin mononucleotide (FMN) (*1*−*3*, *8*), flavin adenine dinucleotide (FAD), and NADPH. An intervening calmodulin binding region (residues 499−530 for iNOS) regulates reduction of NOS_{ox} by NOS_{red} (*8*, *9*). Many structures of mammalian NOS_{ox} proteins ($mNOS_{ox}$) have now been determined in complex with various substrates, cofactors, and inhibitors (*1*). Subunits of $mNOS_{ox}$ homodimers consist of a central winged β-structure surrounded by α-helices (*10*−*13*). The subunits associate at an extensive dimer interface involving both amino- and carboxyl-terminal elements of the polypeptide (*11*−*13*). The

[†] This work was supported by a New Faculty grant from the Camille and Henry Dreyfus Foundation to B.R.C. and by a National Institutes of Health Grant (CA53914) to D.J.S.

[‡] Protein Data Bank entries for reported structures: 1M7V for bsNOS with L-Arg and THF and 1M7Z bsNOS with NHA and THF.

* To whom correspondence should be addressed. Telephone: (607) 254-8634. Fax: (607) 255-1248. E-mail: bc69@cornell.edu.

[§] Cornell University.

[||] The Cleveland Clinic.

[1] Abbreviations: bsNOS, *B. subtilis* NOS; deiNOS, *D. radiodurans* NOS; DHF, dihydrofolate; eNOS, endothelial nitric oxide synthase; FAD, flavin adenine dinucleotide; FMN, flavin mononucleotide; GTP, guanosine triphosphate; H_4B, (6*R*,1′*R*,2′*S*)-5,6,7,8-tetrahydrobiopterin; iNOS, inducible nitric oxide synthase; $iNOS_{ox}$, inducible nitric oxide synthase oxygenase domain; L-Arg, L-arginine; L-Cit, L-citrulline; $mNOS_{ox}$, mammalian nitric oxide synthase oxygenase domain (eNOS, iNOS, or nNOS); NADPH, nicotinamide adenine dinucleotide phosphate; NHA, N^{ω}-hydroxy-L-arginine; nNOS, neuronal nitric oxide synthase; NO, nitric oxide; NOS, nitric oxide synthase; NOS_{red}, nitric oxide synthase reductase domain; pABA, *p*-aminobenzoic acid; THF, tetrahydrofolate (5,6,7,8-tetrahydropteroyl-L-glutamic acid).

10.1021/bi0263715 CCC: $22.00
Published on Web 08/21/2002

active center channel of $iNOS_{ox}$ begins near the dimer interface and leads along the pterin-binding site to the guanidinium-binding site beside the heme iron.

In contrast, bacterial NOS proteins are much smaller than their mammalian counterparts (typically ~360 residues) and only conserve core regions of NOS_{ox} that include binding sites for heme and substrate, but only partial binding sites for pterin (*14*). The bacterial NOSs appear to be missing not only a linked reductase domain but also N-terminal regions of $mNOS_{ox}$ that are important for binding the dihydroxypropyl side chain of H_4B, a zinc ion, and the adjacent subunit of the dimer (*11*−*13*, *15*−*17*).

The pterin cofactor H_4B has been implicated as an electron donor in both steps of the NOS chemical mechanism (*18*−*22*). In the first step, L-Arg is hydroxylated to NHA by a mixed-function oxidation (*2*, *3*, *8*, *18*) analogous to oxygenation reactions catalyzed by the cytochrome P450s (*23*, *24*). In the second step, NHA is converted to L-Cit and NO in an O_2-dependent oxidation that probably involves attack of peroxo-iron [P-Fe(III)-OO^{2-}] on the NHA oxime (R_2-C═N-OH). Both steps require two electrons from an associated reductase domain; however, transient oxidation of H_4B likely delivers the second electron to rapidly activate the heme−oxy complex for both L-Arg and NHA oxidation (*20*−*22*).

NOS-like proteins from *Deinococcus radiodurans* (deiNOS) and *Bacillus subtilis* (bsNOS) have recently been cloned, expressed in *Escherichia coli*, and shown to have NO synthase activity (*14*, *25*). Both proteins are dimers and capable of producing citrulline and NO or NO-derived products from L-Arg in reactions that are dependent on heme, H_4B, and electrons supplied from a surrogate mammalian NOS_{red}. For bsNOS, H_4B was necessary for NO production from NHA (*25*). The rate of heme Fe(II)−O_2 decay also correlated directly with the extent of NO formation and increased substantially in the presence of H_4B (*25*). Curiously, some Gram-positive bacteria such as *D. radiodurans* appear to lack the enzymes to make H_4B (*26*); however, another reduced pteridine produced by bacteria, tetrahydrofolate (THF), will support NO synthesis from both *B. subtilis* and *D. radiodurans* NOS proteins (*14*, *25*).

Herein, we present crystallographic structures of bsNOS with L-Arg and NHA to 1.9 and 2.2 Å resolution, respectively. The absence of key mammalian N-terminal hook, zinc, and pterin-bindng regions has little effect on the bsNOS dimer core. Complexes with the substrates L-Arg and NHA reveal a heme center that is similar to $mNOS_{ox}$, with the exception of a few residue changes in the immediate heme pocket that may explain differences in catalytic parameters between the mammalian and bacterial enzymes. Changes in surface residue conservation implicate a common region for reductase interactions among bacterial and mammalian proteins and compensate for different pterin binding modes between the two classes of NOS.

EXPERIMENTAL PROCEDURES

Materials. Polyethylene glycol was obtained from Hampton and Tris (hydroxymethyl)aminomethane buffer from Fisher Scientific. All other chemicals were from Sigma-Aldrich unless otherwise noted.

Protein Expression and Purification. Full-length *B. subtilis* NOS proteins were PCR cloned into pet15B (Novagen) and overexpressed in *E. coli* BL21(DE3) cells with fused His_6 tags. Proteins were purified in the presence of L-Arg using Ni-chelate chromatography and then size-exclusion chromatography after removal of the His tag with thrombin. Because the transcriptional start site of the *B. subtilis* NOS protein was ambiguous, bsNOS was expressed from a series of constructs that extended the N-terminus beyond the genome-annotated start site (bsNOS+0) (*27*). We found a dramatic effect of N-terminal start position on protein solubility and stability (bsNOS+0, insoluble; bsNOS+7, insoluble; bsNOS+17, insoluble; bsNOS+23, 45 mg/mL; bsNOS+28, 30 mg/mL, and bsNOS+33, 10 mg/mL). Diffraction quality bsNOS crystals where grown from bsNOS+23, the N-terminus of which will hereafter be designated as residue 1.

Table 1: Data Collection and Refinement Statistics for the $bsNOS_{ox}$ Complexes with L-Arg and THF or NHA and THF

	L-Arg and THF	NHA and THF
no. of residues	363	363
cofactor	THF	THF
ligand	L-Arg	NHA
no. of waters	204	204
resolution (Å)	1.94 (1.98−1.94)[g]	2.13 (2.20−2.13)[g]
no. of unique reflections	44343	37880
no. of observations	395408	199903
% completeness	99.7 (99.7)[g]	99.4 (99.2)[g]
$\langle I/\sigma I\rangle$[a]	27.5 (2.5)[g]	10.1 (2.2)[g]
R_{sym}[b] (%)	5.9 (39.9)[g]	8.6 (46.7)[g]
R[c] (%)	22.5 (32.2)	21.2 (32.1)
R_{free}[d] (%)	23.9 (33.3)	23.9 (35.5)
overall $\langle B\rangle$[e] (Å^2)	44.6	43.4
main chain $\langle B\rangle$ (Å^2)	43.3	42.1
side chain $\langle B\rangle$ (Å^2)	44.7	44.2
rmsd for bonds[f] (Å)	0.012	0.012
rmsd for angles[f] (deg)	1.51	1.51

[a] Intensity of the signal to noise ratio. [b] $R_{sym} = \sum\sum_j|I_j - \langle I\rangle|/\sum\sum_j I_j$. [c] $R = \sum||F_{obs}| - |F_{calc}||/\sum|F_{obs}|$ for all reflections (no σ cutoff). [d] R_{free} calculated against 10% of the reflections removed at random. The same free reflections were chosen for all three structures. [e] Overall model average thermal (B) factor. [f] Root-mean-square deviations from bond and angle restraints. [g] Highest-resolution bin for compiling statistics.

Crystallization. Orthorhombic bsNOS crystals of space group $P2_12_12$ (cell dimensions of 81.1 Å × 93.1 Å × 62.0 Å, one NOS subunit per asymmetric unit) were grown in 22−24 h at 22 °C by vapor diffusion from 45 mg/mL protein that had been complexed with freshly dissolved cofactors and substrates at 1−2 mM. L-Arg was removed by dialysis to introduce NHA. THF was dissolved in DMSO to a final concentration of 33 mM and then diluted 26-fold into an NOS protein solution immediately prior to crystallization. Initial crystals grew from drops containing an equal volume mixture of crystallization reservoir and 50 mM Tris (pH 7.5), 150 mM NaCl, and 2 mM dithiothreitol. The reservoir was composed of 100 mM sodium cacodylate (pH 6.0−6.8), 200 mM potassium acetate, and 16−21% polyethylene glycol (PEG) 8K. Nucleated crystals were then seeded into sitting drop solutions of 3−8% PEG 8K (pH 6.5) to produce diffraction quality crystals ranging from 100 to 700 μm in size.

Structure Determination. Diffraction data were collected at 100 K with synchrotron radiation (λ = 0.916 Å) on beamline F-1 of the Cornell High Energy Synchrotron Source (CHESS). The data sets were reduced with DENZO (*28*) and scaled with SCALEPACK (*28*) (Table 1). Initial phases were determined by molecular replacement [AMoRe (*29*)]

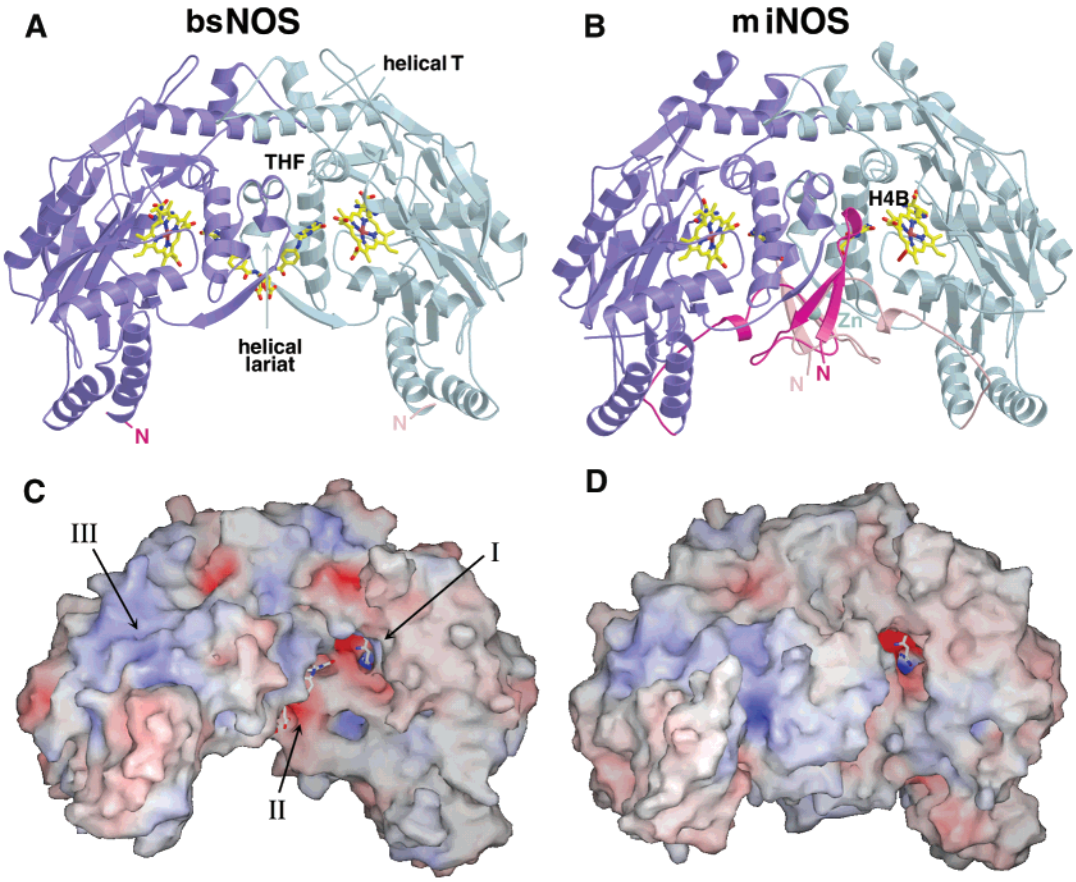

FIGURE 1: Overall structures and surface properties of bsNOS (left) and murine $iNOS_{ox}$ (right). (A and B) The bsNOS and $iNOS_{ox}$ subunits (purple and gray ribbons) associate by interactions of their respective helical lariat and helical T regions to form similar dimers. The N-terminal hook, pterin-binding segment, and zinc site of $mNOS_{ox}$ (magenta and pink ribbons and gray Zn) are absent in the bacterial proteins, allowing for greater exposure of THF (yellow) in bsNOS than of H_4B (yellow) in $mNOS_{ox}$. (C and D) Solvent accessible surfaces for bsNOS and $iNOS_{ox}$ colored by electrostatic potential. In the heme pocket, Ile214 and His124 generate a tighter surface beside the substrate guanidinium in bsNOS than in $iNOS_{ox}$ that limits access to the heme-bound ligands (region I). The THF side chain in bsNOS is also much more exposed than the H_4B side chain in iNOS (blocked from view by the N-terminal hook). A negative electrostatic potential (red) surrounds the THF glutamate group (region II), perhaps contributing to the disorder of the THF side chain. A positive electrostatic potential (blue) on the surface of both bsNOS and $iNOS_{ox}$ surrounds the exposed heme edge (region III). Full saturation of blue or red represents electrostatic potential contoured at ±15 kT/q.

with a probe derived from one subunit of the $iNOS_{ox}\Delta65$ structure (PDB entry 1DWW) with the N-terminal hook and zinc site removed. The model was then automatically rebuilt by ARP-wARP (*30*) and refined in CNS (*31*) using standard positional and thermal factor refinement. Rebuilding with XFIT (*32*) to $F_{obs} - F_{calc}$ and $2F_{obs} - F_{calc}$ maps and addition of pterin, substrates, and water molecules produced the final models (Table 1).

Surface Calculations and Graphics. Molecular surfaces were generated with MS (*33*). Electrostatic potentials were calculated using the linear Possion−Boltzmann equation as implemented in SPOCK (*34*) with the interior protein dielectric set to 4 and the exterior dielectric set to 80. For the potential surfaces that are shown, full charges were used on ionizable residues only; however, calculations carried out with partial charges on all atoms made little difference in the qualitative appearance of the potential maps. MOLSCRIPT (*35*), RASTER3D (*36*), and BOBSCRIPT (*37*) were used to render figures.

RESULTS AND DISCUSSION

Overall Structure and Dimer Stability. The dimeric bsNOS structure is remarkably similar to those of the mammalian NOS_{ox} isozymes ($mNOS_{ox}$), with the exception of an absent N-terminal hook, pterin-binding segment, and zinc-binding site (Figures 1 and 2). The absence of these N-terminal regions reduces the 2115 Å^2 of surface area per subunit buried in the $iNOS_{ox}$ dimer interface to 1115 Å^2 in the bsNOS dimer interface. bsNOS conserves the winged β-sheet core of $mNOS_{ox}$ (*10*), and the absence of the N-terminal hook, zinc, and pterin-binding regions has little effect on conformations or associations of the subunits. This is surprising considering that removal of the first 114 residues from $iNOS_{ox}$ generates a protein ($iNOS_{ox}\Delta114$) that is still longer than the N-terminally truncated bsNOS, but is unstable as a dimer and completely inactive (*38*). Nonetheless, very similar dimer interfaces of bsNOS and $iNOS_{ox}$ with the N-terminal hook removed (Figure 2) indicate that the N-terminal extension of the mammalian enzymes can be viewed as an independent self-interacting module that is not essential for maintaining the structural or catalytic integrity of a NOS subunit core.

Changes in the dimer interface residue composition may manifest differences in dimer stability between bsNOS and $iNOS\Delta114$.[2] One striking difference in the center of the dimer interface is the change of mammalian conserved

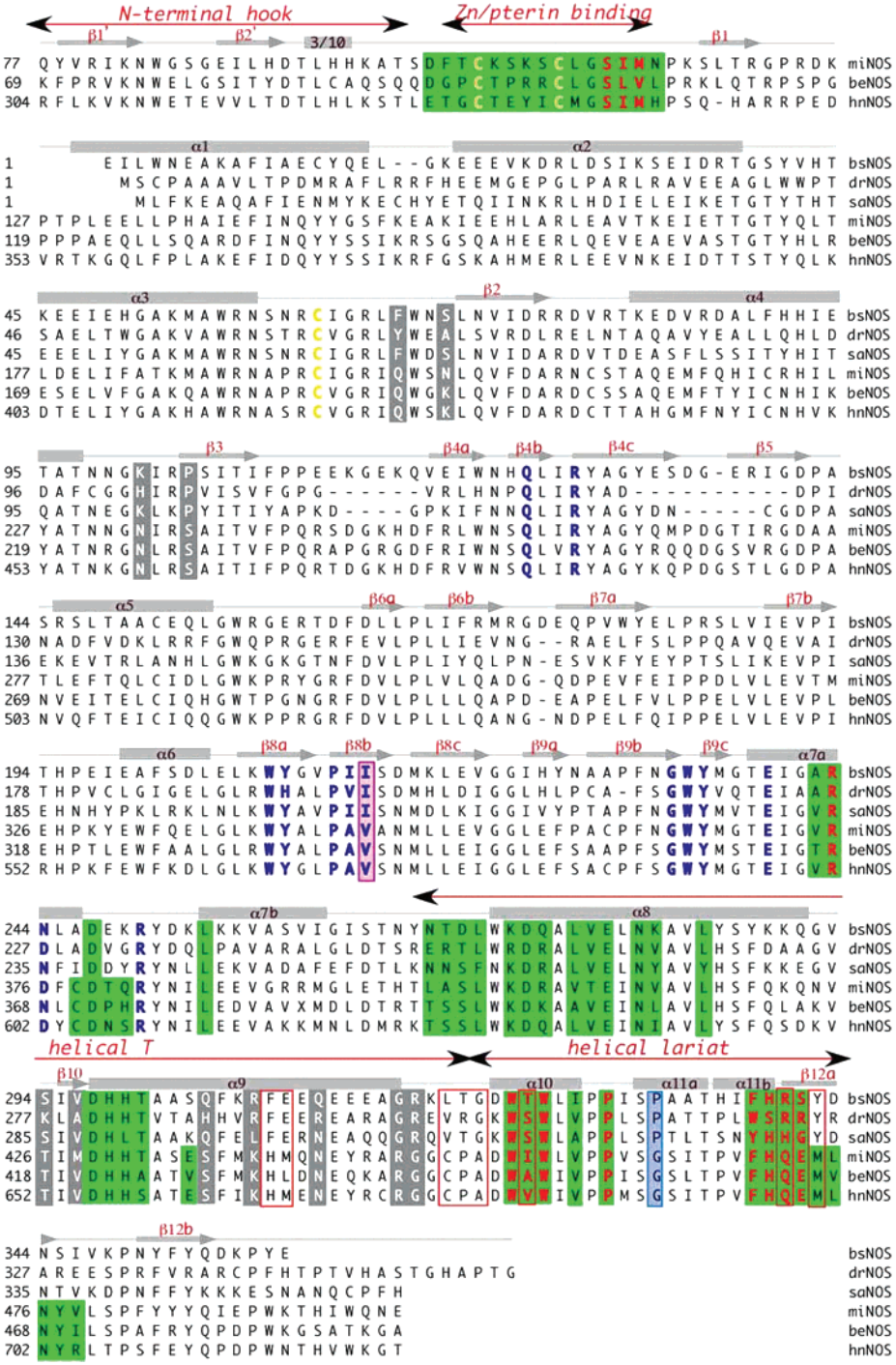

FIGURE 2: Comparison of bacterial and mammalian NOS_{ox} sequences. Sequences for *B. subtilis* bsNOS, *D. radiodurans* drNOS, *S. aureus* saNOS, murine iNOS, bovine eNOS, and human nNOS are color-coded to highlight Cys ligands for binding zinc and heme iron (yellow letters), L-Arg-binding residues (blue letters), and H_4B-binding residues (red letters). Dimer interface residues that contribute at least 5 Å^2 of buried surface area are shown with a green background, whereas a conserved change from Gly to Pro in the center of the dimer interface of bacterial NOSs is shown with a blue background. Residue conservation in bacterial NOSs around the exposed heme edge and causing changes in pterin binding are highlighted by gray backgrounds and red boxes, respectively. A conserved change in the heme pocket from Val to Ile may affect rates of NO dissociation (magenta background). Gray arrows show β-strands, and gray boxes show α-helices; note β11 is omitted because it forms only in the monomeric $iNOS_{ox}\Delta114$ structure (*10*). The protein sequence of bsNOS differs slightly from that reported in the *B. subtilis* genome (*27*).

Gly464 (iNOS) to bacterially conserved Pro332 (bsNOS) (Figure 2). The Pro side chain, which resides on the helical lariat (Figure 1), symmetrically contacts itself across the bsNOS dimer interface and thereby provides an additional hydrophobic contact not possible when Gly occupies this position in $mNOS_{ox}$. Despite this residue substitution, the structural regions composing the dimer interface of bsNOS and either iNOS or eNOS [the helical lariat, helical T, and α7a (*11*); Figures 1 and 2] superimpose well over both subunits of the dimer (0.9 Å rms deviation of Cα positions). The remainder of each subunit pivots against the interface

[2] The additional ~18 N-terminal residues of $iNOS_{ox}\Delta114$ compared to bsNOS may also destabilize the NOS dimer.

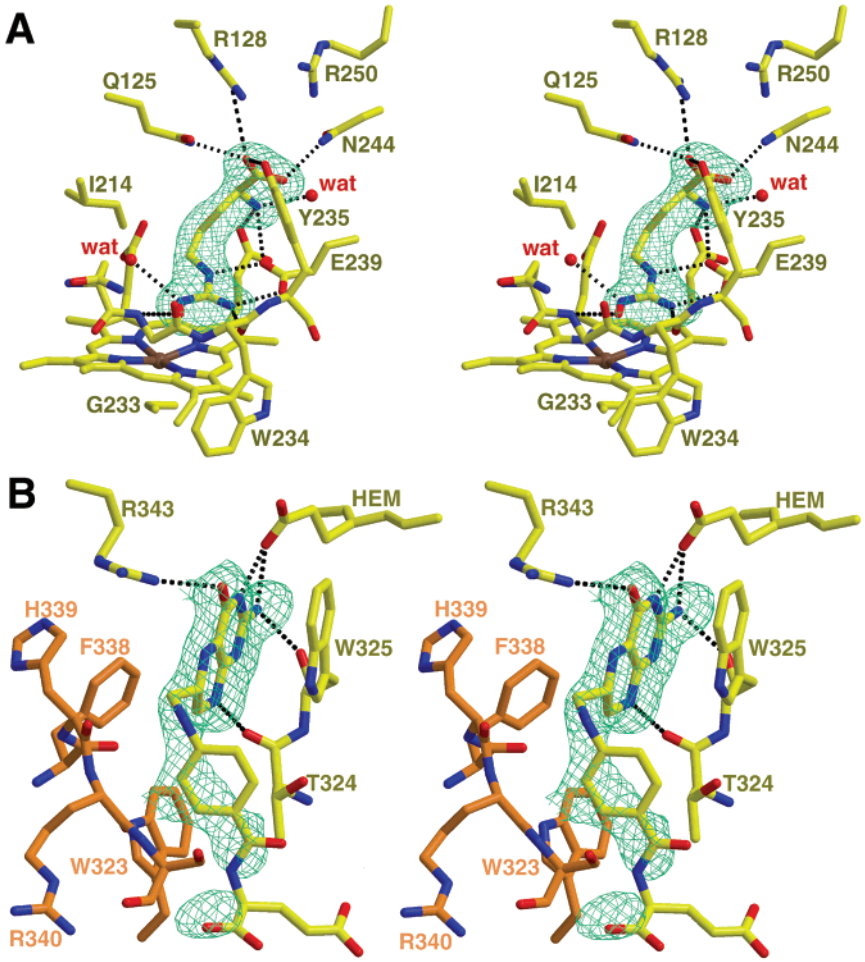

FIGURE 3: Stereoviews of bsNOS binding sites for (A) NHA and (B) THF. (A) The 2.2 Å $F_{obs} - F_{calc}$ omit electron density map for NHA bound in the active center of bsNOS (contoured at 2.5σ). Interactions of NHA with the bsNOS active center (hydrogen bonds shown as black dotted lines) are very similar to those observed in the mammalian NOS−NHA complex, with the exception of Arg128, which does not hydrogen bond to the NHA carboxylate in $mNOS_{ox}$. Water molecules bridge the Pro212 carbonyl (not shown) and the NHA oxime nitrogen and hydrogen bond to the NHA carboxylate. Bacterial NOS proteins also contain Ile214, which will block access to heme-bound ligands from the active center channel. (B) The 2.2 Å resolution $F_{obs} - F_{calc}$ omit electron density map for THF bound in the active center of bsNOS (contoured at 2.5σ). Residues on both subunits of the dimer (yellow and orange side chains) compose the THF binding site. Hydrogen bonds between the pteridine ring and bsNOS are nearly identical to those formed between $mNOS_{ox}$ and H_4B. Low electron density for the THF pABA and glutamate moieties indicates mobility of the THF side chain.

to produce a slight displacement of the peripheral regions in bsNOS compared to $mNOS_{ox}$ (2.0 Å rms deviation of Cα positions over the entire dimer).

Active Center and Substrate Binding. The absence of the N-terminal hook significantly widens the mouth of the substrate access channel compared to $mNOS_{ox}$ (Figure 1). However, the heme pocket, substrate binding sites, and conformations of bound L-Arg and NHA are quite similar in bsNOS and the mammalian enzymes (Figure 3). Thus, it is likely that the natural function of bsNOS is also to oxidize L-Arg to citrulline via NHA.

As in the mammalian NOSs, L-Arg and NHA bind with their guanidinium and hydroxyguanidinium groups stacked between the heme and a Pro side chain (bsNOS 212) (Figures 3A and 4A). The L-Arg and NHA bridging guanidino nitrogen (NE) and one terminal nitrogen (NH1) hydrogen bond to Glu239 and the peptide carbonyl of Trp234 (*11*, *39*). This conformation directs the L-Arg guanidino nitrogen to be hydroxylated (NH2) over the open coordination site of the heme iron where oxygen is activated. As in the mammalian enzymes, pyramidalization of the NHA oxime nitrogen indicates protonation and distorts the hydroxyl from the guanidinium plane (*39*, *40*). The α-amino acid groups of L-Arg and NHA also have analogous interactions with bsNOS as with $mNOS_{ox}$: The amino group hydrogen bonds with Glu239 and the same heme propionate that interacts with the pterin, and the carboxylate group interacts with Tyr235, Asn244, and Gln125 (Figure 3A). Unlike in $mNOS_{ox}$, Arg128 of bsNOS also hydrogen bonds to the substrate carboxylate, whereas the equivalent mNOS residue points away from substrate (Figure 4A). As with $mNOS_{ox}$, the only distinct differences in the binding modes of L-Arg and NHA are the interactions made by the NHA hydroxyl. These include a hydrogen bond from Gly233 to the hydroxyl oxygen that may be important for polarizing the oxime during NO release (*39*).

Other key structural features of the mammalian NO synthase heme centers thought to tune reactivity are also found in the bsNOS enzymes. On the heme proximal side, two pyrrole heme rings bend toward substrate, thereby favoring the nonplanar, protonated configuration of the NHA oxime (*39*). On the heme proximal side, conserved Trp56 stacks with the heme and hydrogen bonds to the iron-

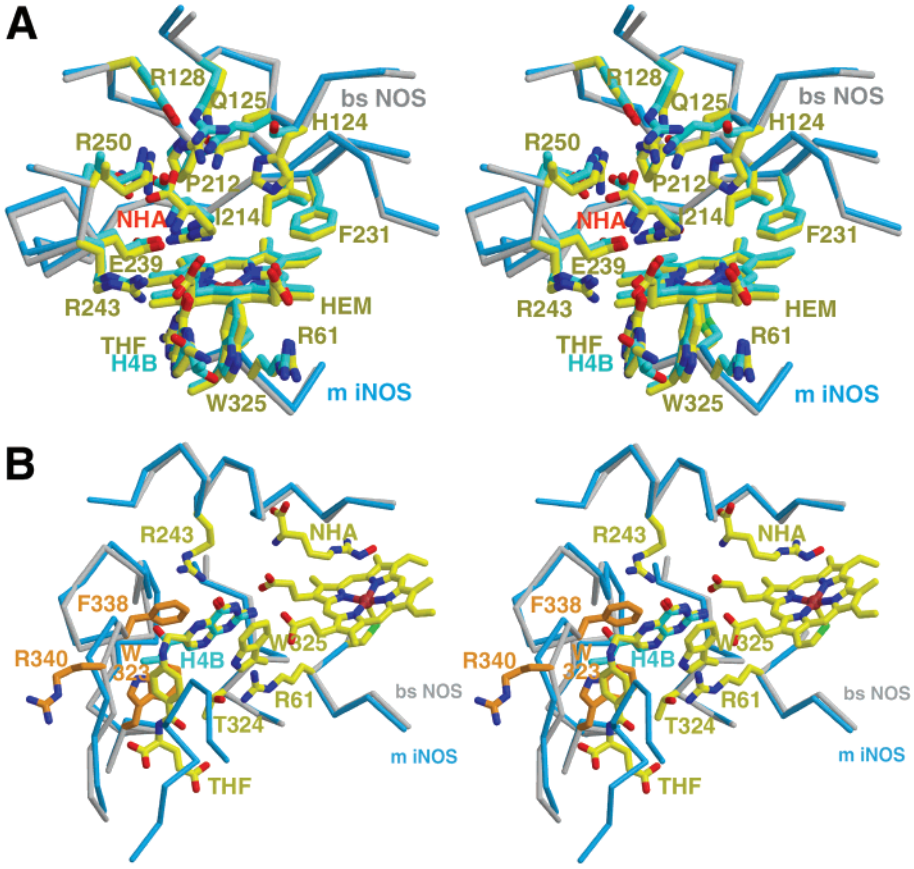

FIGURE 4: Stereoviews of the bsNOS active center. (A) Differences in the heme pocket between bsNOS and $iNOS_{ox}$. The heme pockets of bsNOS (gray Cα trace, yellow side chains and cofactors) and $iNOS_{ox}$ (blue Cα trace, cyan side chains and cofactors) are similar with the exception of Ile214 and His124, which constrain the active center channel in bsNOS. (B) Differences in pterin binding between bsNOS and $iNOS_{ox}$. Superposition of the THF site in bsNOS (yellow pterin, gray Cα trace, yellow and orange side chains for the two subunits of the bsNOS dimer) and the H_4B site in $iNOS_{ox}$ (cyan pterin, blue Cα trace). A conserved change to Arg at position 340 in bacterial NOSs moves β12 toward the pterin and precludes the $mNOS_{ox}$ H_4B side chain conformation but accommodates the side chain linkage of THF. Trp323 contacts the pABA moiety, but the aromatic rings are not well-stacked. Bacterially conserved Thr324 has no hydrogen bonding partners but is in the proximity of the THF amide linkage.

coordinating Cys63. In $mNOS_{ox}$, this hydrogen bond to the Cys thiolate stabilizes heme−NO complexes and probably increases the heme redox potential (*41*−*43*).

Heme Pocket and NO Release. The product NO coordinates the heme Fe(III) at the end of the NOS catalytic cycle (*44*). To release NO from the enzyme and not a byproduct of NO oxidation, NO dissociation from heme must occur before Fe(III) is reduced again to Fe(II) (*45*, *46*). The greatest difference in catalytic parameters between bsNOS and $mNOS_{ox}$ is a 10−20-fold slower dissociation rate for NO from the ferric heme iron at the completion of the reaction cycle (*25*). Interestingly, the bacterial enzymes conserve an Ile or Met (bsNOS Ile214) that projects down from the winged β-sheet alongside the open coordination site of the heme (Figure 4A). In contrast, a smaller Val residue is conserved at this position by $mNOS_{ox}$. As an Ile, this residue will contact NO when it is bound to the heme iron (*47*) and block access of heme ligands to solvent when substrates or products are present (Figures 1C,D and 4A). This greater level of protection of the immediate heme pocket from solvent may stabilize an ordered water molecule that bridges the L-Arg guanidino nitrogen to the Pro212 carbonyl in both bsNOS and $iNOS_{ox}$, but the NHA oxime nitrogen only in bsNOS (*39*). A hydrogen bond from this water molecule to heme-bound NO may also influence heme−NO stability (*48*). Juxtaposed with Ile214, His124 in bsNOS more effectively occludes the channel than the Ser residue found conserved by $mNOS_{ox}$ (Figure 4A). Thus, the bacterial NOS proteins may conserve larger residues at positions 214 and 124 to retain NO longer on the heme or otherwise protect the heme pocket from solvent. As rates of heme and heme−oxy reduction must be carefully timed against NO heme dissociation rates for the mammalian enzymes to produce NO and not NO^- or NO^+ (*45*, *46*), this difference in activity may reflect a function for NOS in bacteria that is distinct from that in mammals.

Pterin Binding. Although the *B. subtilis* genome appears to contain all enzymes needed to synthesize H_4B from GTP (*27*), the genomes of some NOS-containing bacteria such as *D. radiodurans* do not have strong homologues for some of the key enzymes in the H_4B biosynthetic pathway (*26*). H_4B will bind and activate bsNOS with affinity constants commensurate with those for mammalian NOSs (K_D = 0.1 vs 0.03−1 μM) (*25*). Another universally essential tetrahydropteridine, THF, will also bind (K_D = 0.4 μM) and activate bsNOS, but not $mNOS_{ox}$ (*25*). THF has a much larger glutamyl *p*-amino benzoic acid (pABA) side chain than the dihydroxypropyl side chain of H_4B. In $mNOS_{ox}$, N-terminal residues, absent in bsNOS, interact with the H_4B dihydroxylpropyl side chain and sequester the distal end of the pteridine

ring from solvent (Figures 1, 2, and 4). Interactions provided to the pteridine ring by bsNOS are otherwise similar to those provided by the $mNOS_{ox}$ core subunit, and the amount of pteridine surface area buried by each class of NOS does not greatly differ (54.7 Å^2 for bsNOS and 36.7 Å^2 for $iNOS_{ox}$) (Figures 3B and 4B). Nonetheless, given that mammalian conserved interactions between the H_4B side chain and the N-terminal pterin-binding segment are lost by the bacterial enzymes, it is surprising that the affinity of bsNOS for H_4B rivals that of the mammalian enzymes (*25*). Importantly, interactions that are key for the pterin in donating electrons to the heme are maintained in bsNOS. A hydrogen bond between a heme carboxylate and the 3,4-amide of the pterin electronically couples the two cofactors (*11*, *12*, *39*), and Trp325 (iNOS 457) stacks with the pterin to control its redox properties (*49*, *50*) (Figures 3B and 4).

Low electron density for the THF side chain in our structures indicates that bsNOS alone does not provide a strong binding site for THF[3] (Figure 3B). This is likely attributed to poor electrostatic complementation for the THF glutamate in the bsNOS pterin-binding pocket[4] (Figure 1C). Both THF glutamate moieties in the bsNOS dimer lie close to each other in a negatively charged region on the protein surface generated in part by Asp322 and Asp343 (Figure 1C). Interestingly, this same region in deiNOS is predicted to be rich in positively charged residues (Asp322, Asp343, and Ser345 in bsNOS are replaced with Lys305, Arg326, and Arg328 in deiNOS, Figure 2). Thus, deiNOS may be better suited for binding the THF side chain than bsNOS.

Conserved residue differences in bacterial NOS proteins compared to their mammalian counterparts suggest that the bacterial enzymes have evolved to recognize pterin side chains in a manner that differs from that of $mNOS_{ox}$. A bacterially conserved change at residue 340 to Arg (bsNOS) from Gln($mNOS_{ox}$) shifts the β12 peptide backbone toward the smaller THF side chain linkage and also sterically disfavors the dihydroxypropyl side chain conformation found for H_4B in $mNOS_{ox}$ (Figures 3B and 4B). In bsNOS, Arg340 salt bridges with α9 residue Glu309, which is also a conserved change in bacterial NOSs from the Met or Leu residues found in $mNOS_{ox}$. A series of other conserved residues found only in bacterial NOSs on α9, α10, and β12 compensate for the addition of Arg340 and Glu309 (Figure 2). Notably, bacterially conserved Thr(Ser)324, which is an Ile in $mNOS_{ox}$, provides a hydroxyl group in the bsNOS pterin-binding site that does not hydrogen bond with THF and does not seem to be well-positioned to hydrogen bond with H_4B. Thus, although our structures suggest that bsNOS alone does not contain an optimized binding site for THF, residue changes in the pterin site conserved among bacterial NOSs indicate that either the H_4B side chain binds bsNOS in a mode that differs from that of $mNOS_{ox}$ (perhaps involving another protein) or a somewhat different cofactor is the natural target of this site.

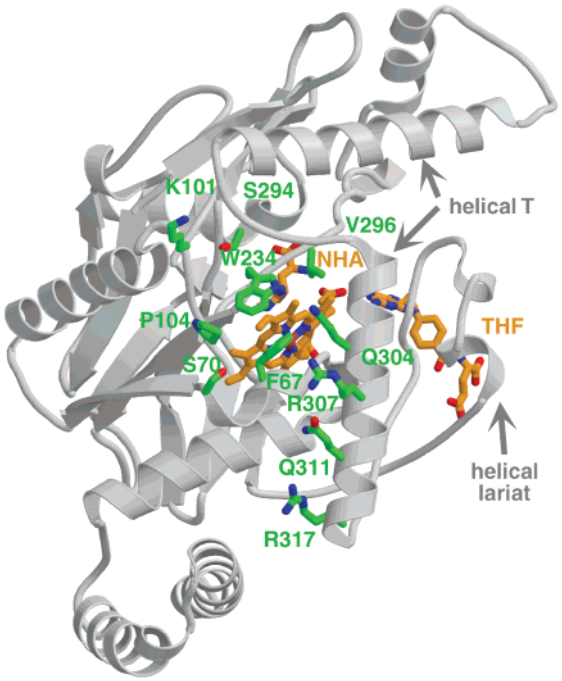

FIGURE 5: Surface patch for potential reductase protein interactions in bacterial and mammalian NOSs. One subunit of the bsNOS dimer shown as a gray ribbon diagram. Residues (green) surrounding the exposed heme edge (orange) in bsNOS are conserved in bacterial NOS proteins (see Figure 2). This surface patch corresponds to region III of panels C and D of Figure 1.

Interaction Surfaces and Partner Proteins. Mammalian NOS proteins require a reductase domain to provide electrons for reducing both the heme center and the pterin. We have previously suggested that a surface patch of conserved residues surrounding an exposed heme edge of the mammalian NOSs may mediate reductase interactions (*11*, *16*). Some of these key positions have residues that are conserved by both mammalian and bacterial NOSs (Trp234, Val296, Arg307, Gln311, and Arg317), whereas others are conserved only by the bacterial enzymes (Phe67, Ser70, Lys101, Pro104, and Gln304) (Figures 2 and 5). Particularly striking is a mammalian conserved Arg at the base of α9 (iNOS 448) not conserved in sequence by the bacterial enzymes but in topographical position by the bsNOS structure: The Arg448-Gly449 dipeptide in $mNOS_{ox}$ corresponds to the reverse sequence Gly316-Arg317 in bsNOS (Figure 2), but in bsNOS, these residues flip conformation to maintain the exposure of Arg317. This Arg (bsNOS 317 and iNOS 448) contributes to a positive electrostatic potential on the conserved surface patch of both $iNOS_{ox}$ and bsNOS (Figure 1C,D, region III).

The molecular surface surrounding the exposed heme edge of NOS_{ox} may indeed mediate interactions with reductase proteins in both prokaryotes and mammals, but the residue makeup of these interfaces will be somewhat different between bacterial and mammalian NOSs. Nonetheless, a surrogate mammalian reductase protein will drive bsNOS and deiNOS to synthesize NO from L-Arg, and deiNOS forms heterodimers with full-length mammalian subunits that

[3] The THF used in these studies is a mixture of the natural 6*S* and unnatural 6*R* stereoisomers. Despite low electron density for the THF side chain, refinement of (6*S*)-THF, (6*R*)-THF, and dihydrofolate in the bsNOS pterin site favors the 6*S* conformation due to unfavorable contacts of the other two pterins with the peptide backbone of β12. Crystals of THF-bound bsNOS were also grown and flash-cooled in liquid N_2 under strict anaerobic conditions to limit oxidation of THF to DHF. Pterin electron density from crystals treated anaerobically is identical to that shown in Figure 3B.

[4] Slightly different conformations for the THF glutamate in the L-Arg and NHA bsNOS structures are indicated by the weak electron density observed in this region. However, both structures suggest a hydrogen bond between the glutamate amino acid carboxylate and the peptide nitrogen of Tyr342 on the adjacent subunit.

are active in electron transfer (ET) (*14*, *25*). Thus, conservation of the positive surface potential (Figure 1C) may impart some overlap in reductase recognition properties for mammalian and bacterial NOS_{ox}. The ability of $nNOS_{red}$ to reduce bsNOS also emphasizes the fact that a zinc center is unlikely to be essential for catalysis-supporting ET into NOS_{ox}. Whether the N-terminal hook is expendable for ET and NOS_{red} interactions is less clear because in heterodimer systems bacterial NOSs could receive an N-terminal hook from the mammalian subunit via a domain swapping interaction that has been observed in $iNOS_{ox}$ under some conditions (*16*, *17*). The *B. subtilis* genome does contain sequences for flavoproteins homologous to mammalian NOS reductase domains, although these proteins are absent in *D. radiodurans* (*26*, *27*). Thus, although some commonalities are expected, the identity, role, and perhaps even necessity of NOS reductase partners may vary considerably among different organisms.

Looking Ahead. Finally, the biological role of NO production by NOS in bacteria is currently unknown. Given the reactivity of nitric oxide and its diverse activities in mammals, the prevalence of NOS proteins in the prokaryotic kingdom is certainly intriguing. The increased stability of the NO−heme complex in bsNOS that correlates with residue changes in the heme pocket that are conserved among the bacterial enzymes suggests that a slower release of NO from the synthase may be important for function. We note that although there is yet no link to disease, human pathogens such as *Staphylococcus aureus* and *Bacillus anthracis* (Anthrax) contain proteins very similar to bsNOS. If these enzymes are essential for viability or pathogenicity, lessons learned from the structure-based design of inhibitors targeting the mammalian NOS enzymes may be applicable to combating infectious agents. Fortunately, the noted structural differences in the immediate heme pocket, pterin site, and substrate access channel should allow inhibitor discrimination between mammalian and bacterial NOS proteins.

ACKNOWLEDGMENT

We thank CHESS for access to data collection facilities, Cristian Gradinaru and Sang-Youn Park for help with data collection and computation, and J. A. Tainer and E. D. Getzoff for encouraging the bacterial NOS structure project in our laboratory.

REFERENCES

1. Alderton, W. K., Cooper, C. E., and Knowles, R. G. (2001) *Biochem. J. 357*, 593.
2. Pfeiffer, S., Mayer, B., and Hemmens, B. (1999) *Angew. Chem., Int. Ed. 38*, 1715.
3. Griffith, O. W., and Stuehr, D. J. (1995) *Annu. Rev. Physiol. 57*, 707.
4. Stuehr, D. J., Kwon, N. S., Nathan, C. F., Griffith, O. W., Feldman, P. L., and Wiseman, J. (1991) *J. Biol. Chem. 266*, 6259.
5. Cutruzzola, F. (1999) *Biochim. Biophys. Acta 1411*, 231.
6. Choi, W. S., Chang, M. S., Han, J. W., Hong, S. Y., and Lee, H. W. (1997) *Biochem. Biophys. Res. Commun. 237*, 554.
7. Chen, Y. J., and Rosazza, J. P. N. (1995) *J. Bacteriol. 177*, 5122.
8. Masters, B. S. S., McMillan, K., Sheta, E. A., Nishimura, J. S., Roman, L. J., and Martasek, P. (1996) *FASEB J. 10*, 552.
9. Stuehr, D. J. (1997) *Annu. Rev. Pharmacol. Toxicol. 18*, 707.
10. Crane, B. R., Arvai, A. S., Gachhui, R., Wu, C., Ghosh, D. K., Getzoff, E. D., Stuehr, D. J., and Tainer, J. A. (1997) *Science 278*, 425.
11. Crane, B. R., Arvai, A. S., Ghosh, D. K., Wu, C., Getzoff, E. D., Stuehr, D. J., and Tainer, J. A. (1998) *Science 279*, 2121.
12. Raman, C. S., Li, H., Martasek, P., Kral, V., Masters, B. S. S., and Poulos, T. L. (1998) *Cell 95*, 939.
13. Fischmann, T. O., Hruza, A., Niu, X. D., Fossetta, J. D., Lunn, C. A., Dolphin, E., Prongay, A. J., Reichert, P. R., Lundell, D. J., Narula, S. K., and Weber, P. C. (1999) *Nat. Struct. Biol. 6*, 233.
14. Adak, S., Bilwes, A. M., Panda, K., Hosfield, D., Aulak, K. S., McDonald, J. F., Tainer, J. A., Getzoff, E. D., Crane, B. R., and Stuehr, D. J. (2002) *Proc. Natl. Acad. Sci. U.S.A. 99*, 107.
15. Li, H., Raman, C. S., Glaser, C. B., Blasko, E., Young, T. A., Parkinson, J. F., Whitlow, M., and Poulos, T. (1999) *J. Biol. Chem. 30*, 21276.
16. Crane, B. R., Rosenfeld, R., Arvai, A., Ghosh, D., Ghosh, S., Tainer, J. A., Stuehr, D. J., and Getzoff, E. D. (1999) *EMBO J. 18*, 6271.
17. Ghosh, D. K., Crane, B. R., Ghosh, S., Wolan, D., Gachhui, R., Crooks, C., Presta, A., Tainer, J. A., Getzoff, E. D., and Stuehr, D. J. (1999) *EMBO J. 18*, 6260.
18. Groves, J. T., and Wang, C. C. Y. (2000) *Curr. Opin. Chem. Biol. 4*, 687.
19. Gorren, A. C. F., and Mayer, B. (2002) *Curr. Drug Metab. 3*, 133.
20. Adak, S., Wang, Q., and Stuehr, D. J. (2000) *J. Biol. Chem. 275*, 33554.
21. Wang, Z. Q., Wei, C. C., and Stuehr, D. J. (2002) *J. Biol. Chem. 277*, 12830.
22. Hurshman, A. R., and Marletta, M. A. (2002) *Biochemistry 41*, 3439.
23. Mueller, E. J., Loida, P. J., and Sligar, S. G. (1995) in *Cytochrome P450: Structure, Mechanism, and Biochemistry* (de Montellano, P. R. O., Ed.) pp 83−124, Plenum Press, New York.
24. Sono, M., Roach, M. P., Coulter, E. D., and Dawson, J. H. (1996) *Chem. Rev. 96*, 2841.
25. Adak, S., Aulak, K., and Stuehr, D. (2002) *J. Biol. Chem. 277*, 16167.
26. White, O., Eisen, J., Heidelberg, J., Hickey, E., Peterson, J., Dodson, R., Haft, D., Gwinn, M., Nelson, W., Richardson, D., Moffat, K., Qin, H., Jiang, L., Pamphile, W., Crosby, M., Shen, M., Vamathevan, J., Lam, P., McDonald, L., Utterback, T., Zalewsk, C., Makarova, K., Aravind, L., Daly, M., Minton, K., Fleischmann, R., Ketchum, K., Nelson, K., Salzberg, S., Smith, H., Venter, J., and Fraser, C. (1999) *Science 286*, 1571.
27. Kunst, F., Ogasawara, N., Moszer, I., Albertini, A., Alloni, G., Azevedo, V., Bertero, M., Bessieres, P., Bolotin, A., Borchert, S., Borriss, R., Boursier, L., Brans, A., Braun, M., Brignell, S., Bron, S., Brouillet, S., Bruschi, C., Caldwell, B., Capuano, V., Carter, N., Choi, S., Codani, J., Connerton, I., and Danchin, A. (1999) *Nature 390*, 249.
28. Otwinowski, Z. (1993) in *Data Collection and Processing* (Sawyer, L., Isaacs N., and Bailey, S., Eds.) pp 56−62, Science and Engineering Research Council, Warrington, U.K.
29. Navaza, L. (1994) *Acta Crystallogr. A50*, 157.
30. Perrakis, A., Sixma, T., Wilson, K. S., and Lamzin, V. S. (1997) *Acta Crystallogr. D53*, 448.
31. Brünger, A. T., Adams, P. D., Clore, G. M., DeLano, W. L., Gros, P., Grosse-Kunstleve, R. W., Jiang, J. S., Kuszewski, J., Nilges, M., Pannu, N. S., Read, R. J., Rice, L. M., Simonson, T., and Warren, G. L. (1998) *Acta Crystallogr. D54*, 905.
32. McRee, D. E. (1992) *J. Mol. Graphics 10*, 44.
33. Connolly, M. L. (1983) *Science 221*, 709.
34. Christopher, J. (1998) *J. Mol. Graphics 16*, 285.
35. Kraulis, P. (1991) *J. Appl. Crystallogr. 24*, 946.
36. Merritt, E., and Bacon, D. (1997) *Methods Enzymol. 277*, 505.
37. Esnouf, R. (1997) *J. Mol. Graphics 15*, 133.
38. Ghosh, D. K., Wu, C., Pitters, E., Moloney, M., Werner, E. R., Mayer, B., and Stuehr, D. J. (1997) *Biochemistry 36*, 10609.
39. Crane, B. R., Arvai, A. S., Ghosh, S., Getzoff, E. D., Stuehr, D. J., and Tainer, J. A. (2000) *Biochemistry 39*, 4608.
40. Tierney, D. L., Huang, H., Martasek, P., Masters, B. S. S., Silverman, R. B., and Hoffman, B. M. (1999) *Biochemistry 38*, 3704.
41. Couture, M., Adak, S., Stuehr, D. J., and Rousseau, D. L. (2001) *J. Biol. Chem. 276*, 38280.
42. Adak, S., Wang, Q., and Stuehr, D. J. (2000) *J. Biol. Chem. 275*, 17434.

43. Adak, S., Crooks, C., Wang, Q., Crane, B. R., Tainer, J. A., Getzoff, E. D., and Stuehr, D. J. (1999) *J. Biol. Chem. 274*, 26907.
44. Wang, J., Rousseau, D. L., Abu-Soud, H. M., and Stuehr, D. J. (1994) *Proc. Natl. Acad. Sci. U.S.A. 91*, 10512.
45. Santolini, J., Adak, S., Curran, C. M. L., and Stuehr, D. J. (2001) *J. Biol. Chem. 276*, 1233.
46. Santolini, J., Meade, A. L., and Stuehr, D. J. (2001) *J. Biol. Chem. 276*, 48887.
47. Li, D., Couture, M., Rousseau, D. L., Stuehr, D. J., and Yeh, S. R. (2002) *Biophys. J. 82*, 2185.
48. Olson, J. S., and Phillips, G. (1997) *J. Biol. Inorg. Chem. 2*, 544.
49. Wang, Z. Q., Wei, C. C., Ghosh, S., Meade, A. L., Hemann, C., Hille, R., and Stuehr, D. J. (2001) *Biochemistry 40*, 12819.
50. Aoyagi, M., Arvai, A. S., Ghosh, S., Stuehr, D. J., Tainer, J. A., and Getzoff, E. D. (2001) *Biochemistry 40*, 12826.

BI0263715